Paediatrics Publications   Paediatrics Department

3-1-2012

Differential detection and distribution of microglial and hematogenous macrophage populations in the injured spinal cord of lys-EGFP-ki transgenic mice

Leah A. Mawhinney
Robarts Research Institute

Sakina G. Thawer
Robarts Research Institute

Wei Yang Lu
Western University

Nico Van Rooijen
Vrije Universiteit Amsterdam

Lynne C. Weaver
Robarts Research Institute

See next page for additional authors

Follow this and additional works at: https://ir.lib.uwo.ca/paedpub

Authors

Leah A. Mawhinney, Sakina G. Thawer, Wei Yang Lu, Nico Van Rooijen, Lynne C. Weaver, Arthur Brown, and Gregory A. Dekaban

ORIGINAL ARTICLE

Differential Detection and Distribution of Microglial and Hematogenous Macrophage Populations in the Injured Spinal Cord of *lys*-EGFP-*ki* Transgenic Mice

Leah A. Mawhinney, MSc, MD, Sakina G. Thawer, BSc, MSc, Wei-Yang Lu, PhD, Nico van Rooijen, PhD, Lynne C. Weaver, DVM, PhD, Arthur Brown, PhD, and Gregory A. Dekaban, PhD

Abstract

The acute inflammatory response that follows spinal cord injury (SCI) contributes to secondary injury that results in the expansion of the lesion and further loss of neurologic function. A cascade of receptor-mediated signaling events after SCI leads to activation of innate immune responses including the migration of microglia and active recruitment of circulating leukocytes. Because conventional techniques do not always distinguish macrophages derived from CNS-resident microglia from blood-derived monocytes, the role that each macrophage type performs cannot be assessed unambiguously in these processes. We demonstrate that, in the normal and spinal cord–injured *lys*-EGFP-*ki* transgenic mouse, enhanced green fluorescent protein (EGFP) is expressed only in mature hematopoietic granulomyelomonocytic cells and not in microglia. This allowed us to assess the temporal and spatial relationships between microglia-derived and hematogenous macrophages as well as neutrophils during a period of 6 weeks after clip compression SCI. Within the lesion, EGFP-positive monocyte–derived macrophages were found at the epicenter surrounded by EGFP-negative–activated microglia and microglia-derived macrophages. Neutrophils were not present when EGFP-positive monocyte–derived macrophages were depleted, indicating that neutrophil persistence in the lesion depended on the presence of these monocytes. Thus, these 2 distinct macrophage populations can be independently identified and tracked, thereby allowing their roles in acute and chronic stages of SCI-associated inflammation to be defined.

Key Words: Clodronic acid liposomes, Enhanced green fluorescent protein, Inflammation, Macrophage, Microglia, Spinal cord injury, Transgenic mouse.

INTRODUCTION

The acute inflammatory response that follows mechanical injury to the spinal cord is a major contributor to the secondary injury response and results in expansion of the lesion and further loss of neurologic function. The roles that different inflammatory cells play in spinal cord injury (SCI) remain unclear. Many studies examining ways to block or reduce the acute inflammatory responses to SCI have found that these responses adversely affect neurologic recovery (1–9). However, inflammation is a critical part of the normal wound healing process, and the acute inflammatory response to SCI may also promote recovery (7–13). These seemingly contradictory findings demonstrate that the role of inflammation and, in particular, the phenotype and functional subsets of the responding immune cells need to be defined further, as do their temporal appearance and spatial distribution within the lesion. Without this detailed understanding, effective clinical immunotherapies for SCI cannot be readily developed.

Spinal cord injury results in an inflammatory response that is initiated by the release of proinflammatory mediators from CNS cells resident in or adjacent to the lesion (1, 7, 9). These mediators lead to a sequentially orchestrated activation and migration of microglia toward the lesion and active recruitment of circulating leukocytes to the injury (1, 14). Once in the injured spinal cord, identification and tracking of each type of inflammatory cell can be difficult. Whereas neutrophils are easily distinguished from microglia, macrophages derived from microglia (mMΦ) and those derived from hematogenous monocytes (hMΦ) are not readily discriminated owing to their morphological and phenotypic similarities (15–19). Hence, within the spinal lesion, discerning the spatial distribution and functional roles of these macrophages of different origins becomes a significant challenge (3, 16, 18, 20).

The inability to distinguish between hMΦ and mMΦ after SCI has limited progress in our understanding of their cooperative and antagonistic relationship during wound healing and of temporal variations in that relationship. Previous studies distinguishing mMΦ and hMΦ populations used bone marrow chimeric rats or mice (16, 21–23), whereas other studies used methods to deplete monocytes selectively (3). These

methods require alteration of the leukocyte populations of the animals before SCI that lead to potential difficulties in data interpretation, however (24, 25). An alternative method for distinguishing microglia and mMΦ from monocytes and hMΦ would be advantageous.

Examination of the literature suggested to us that lysozyme M might serve as useful marker to differentiate microglia and hematogenous macrophages (17, 26, 27). This study characterizes the cellular inflammatory events associated with SCI in the lysozyme M–EGFP-knock in (*lys*-EGFP-*ki*) transgenic mouse, a model that we propose for discriminating microglia and mMΦ from monocytes and hMΦ in SCI. In these transgenic mice, the EGFP coding sequence replaces that of lysozyme M and is regulated by the native lysozyme M promoter, which drives the expression of EGFP specifically in mature myelomonocytic cells, including neutrophils, monocytes, and macrophages (28). These *lys*-EGFP-*ki* mice exhibit normal developmental, behavioral, reproductive, and most immunologic characteristics but are more susceptible to certain bacterial infections (28, 29). We previously found that microglia did not express EGFP in the brains of *lys*-EGFP-*ki* mice with experimental autoimmune encephalomyelitis (30). We therefore designed a study to determine whether microglia and mMΦ could be distinguished from hMΦ in a mouse model of SCI. We used a clip compression model because spinal cord compression is a very common feature of human SCI (31). Unlike the more commonly studied contusion mouse models of SCI, clip compression involves an ischemia-reperfusion component of the injury that likely generates a more intense inflammatory response, thereby mimicking a significant sector of the human SCI population (31, 32). We report that EGFP, under the control of the lysozyme M promoter, permits microglia and mMΦ to be distinguished temporally and spatially from neutrophils, monocytes, and hMΦ after SCI.

MATERIALS AND METHODS

Animals

All protocols for this study were approved by the University of Western Ontario Animal Use Subcommittee and conform to the Canadian Council on Animal Care guidelines. The original *lys*-EGFP-*ki* transgenic mice were provided by Dr Thomas Graf (28), from the Albert Einstein College of Medicine (Bronx, NY), and homozygous mice were bred subsequently in the mouse barrier facility at the Robarts Research Institute. Wild-type C57BL/6 mice were obtained from Charles River Laboratories, Wilmington, MA.

Acute Spinal Cord Compression Injury

Mice (20–26 g), 8 to 14 weeks old, underwent experimental clip compression injury at thoracic spinal segment 5 (T5), as previously described (33). Spinal cord injury was performed using a modified aneurysm clip (8 g force) (31). After 60 seconds of compression, the clip was removed, and the surgical area was closed in layers. The force applied to the spinal cord produced a severe SCI and resulted in immediate paraplegia. Postoperatively, the mice with SCI were treated as previously described for rat studies with respect to hydration,

analgesia, and antibiotic therapy (34). Their bladders were emptied by manual compression twice daily for the first 2 weeks after SCI and then as needed.

Clodronic Acid Liposome Treatment

Premade clodronic acid liposomes (Clodronate Liposomes Foundation, Amsterdam, The Netherlands; http://www.clodronateliposomes.org) were administered 24 hours before surgical SCI to deplete macrophages from the blood, bone marrow, spleen, liver, peritoneum, and most lymph nodes. For each treatment, 100 μl/10 g body weight was administered intravenously (i.v.) and 50 μl/10 g intraperitoneally (i.p.). Subsequently, treatments were administered every fourth day for the duration of the experimental period. Enhanced green fluorescent protein–positive leukocytes began to reappear in the blood at this time in significant numbers (data not shown), consistent with previous literature reports (35). Depletion was verified using flow cytometry to assess the peripheral blood leukocytes and splenocytes at the appropriate time points. Mice with depletion greater than 85% to 90% were used.

PKH Liposome Staining

Control phosphate-buffered saline (PBS)–containing liposomes were stained using a PKH26 red fluorescent cell linker kit (Sigma, St Louis, MO) to label the membrane portion of the liposomes. Briefly, the staining procedure was as follows: liposomes were washed with PBS (Gibco Invitrogen Corp, Burlington, Canada) and subjected to ultracentrifugation, and the pellet was resuspended in diluent C provided by the manufacturer. The staining solution, PKH dye in diluent C, was quickly added to the liposomes and incubated for 5 minutes. The staining reaction was stopped with PBS containing 1% bovine serum albumin (BSA; Roche Diagnostics, Basel, Switzerland). The sample was diluted with PBS, centrifuged as previously mentioned, and then washed with PBS. The final pellet was resuspended in PBS and stored at 4°C in the dark. Visual fluorescent microscopic examination verified that all liposomes were stained with PKH26. For each animal, 100 μl/10 g of the PKH-stained liposomes was administered i.v. and 50 μl/10 g i.p. either once at 24 hours before SCI or twice at 24 hours before SCI and 3 days after SCI.

Tissue Preparation

Transcardiac perfusions were performed 1, 3, 4, 7, 14 and 42 days after SCI. All mice were deeply anesthetized with an i.p. injection of ketamine/xylazine and perfused with oxygenated tissue culture medium (pH 7.4, Dulbecco modified Eagle medium; Gibco), followed by 4% paraformaldehyde fixative in 0.1 mol/L phosphate buffer (pH 7.4), both at room temperature. The thoracic region of the spinal cords containing the injury from spinal segments T3 to T6 was removed and fixed overnight at 4°C in 4% formaldehyde. The spinal cords were cryoprotected in increasing concentrations of sucrose in PBS (10%, 20%, and 30%) at 4°C. The spinal cord segments were embedded with Tragacanth tissue gum (Sigma-Aldrich Canada Ltd., Oakville, Canada) made with 30% sucrose or OCT compound (Sakura Finetek, Inc, Torrance, CA); 16- to 20-μm-thick cross sections were cut on a cryostat (Leica CM3050 S; Leica Microsystems Inc., Markham, Canada). Four sets of

alternate sections were mounted onto gel-coated slides and allowed to dry for 24 hours.

Immunofluorescence Microscopy

A double-staining procedure was performed using detergent (quenching EGFP fluorescence) permitting EGFP expression to be assessed quantitatively in sections costained for Ly6/G (granulocytes) or F4/80 (monocyte/MΦ) or with tomato lectin (TL; blood vessels and MΦ). Tissue sections were blocked with 10% normal horse serum (Invitrogen) and 10% normal mouse serum (Jackson ImmunoResearch Laboratories, West Grove, PA) in Tris–phosphate-buffered saline plus 0.3% Triton X-100 (TPBS-X, pH 7.4). The primary antibodies used were biotinylated anti-mouse Ly6/G (1:500; eBioscience, San Diego, CA), F4/80 (Jackson ImmunoResearch Laboratories), and Alexa Fluor 488–conjugated rabbit anti-GFP (1:1000; Molecular Probes, Burlington, Canada). Alternatively, a biotinylated anti-GFP antibody (1:1000; Santa Cruz Biotechnology, Santa Cruz, CA), amplified with biotinylated tyramide, as previously described (36), was used with the Rhodamine Red fluorochrome conjugated to streptavidin (1:200; Jackson ImmunoResearch Laboratories). Anti-human myeloperoxidase (MPO) antibody was used as previously described (34). Biotinylated TL staining (*Lycopersicon esculentum*, 20 μg/mL; Vector Laboratories, Burlington, Canada) was performed according to the manufacturer's instructions with streptavidin Alexa Fluor 594 and then with the Alexa Fluor 488 anti-GFP antibody, as described previously. All washes were performed in 1% normal horse serum plus 1% normal mouse serum in either TPBS-X or TPBS, unless otherwise indicated by the manufacturer. Alternatively, a method was developed for a detergent-free staining procedure using biotinylated anti-mouse CD11b and anti-mouse Ly6/G to preserve EGFP fluorescence. Sections were blocked as described previously and then exogenous biotin was blocked with an avidin/biotin blocking kit (Vector Laboratories). The sections were then incubated for 3 days at 4°C with either biotinylated anti-CD11b (1:200) or biotinylated anti-Ly6/G (1:200) in TPBS, followed by washing in the absence of detergent. Slides were stained with 4',6-diamidino-2-phenylindole (1:1000 in PBS) for 5 minutes, washed with TPBS and finally rinsed with distilled water. The slides were left to dry overnight, and coverslips were mounted with either Vectashield (Vector Laboratories) or Gel/Mount (Biomeda Corp, Foster City, CA).

Quantification of EGFP-Positive and Ly6/G–Positive Cells

To quantify the labeled cells at the injury site, sections from the injured spinal cord were viewed in a blinded fashion using a Bio-Rad Radiance 2000 MP laser scanning 2-photon confocal microscope (Bio-Rad Laboratories, Hertfordshire, UK). Digital images of cross-sectional slices of the spinal cord were acquired using a 10× objective and Laser-Sharp software (Bio-Rad). Eleven sections were quantified from each injured cord. These sections were sampled evenly across the T2–T5 region starting at the section in the middle of the lesion. Five sections spaced 160 μm apart were sampled from

the epicenter of the lesion to spinal segment T3 (rostral) and from the epicenter to spinal segment T5 (caudal). Ly6/G (visualized by Rhodamine Red) and EGFP expressions were quantified separately from the same double-stained sections using quantitative digital morphometry and ImagePro software version 4.5.1.22 (Media Cybernetics, Inc, Silver Springs, MD), as previously described (34). Data are presented as the ratio of the total immunoreactive area to the entire area of the spinal cord section assessed (designated as the area of interest) and represent the relative amount of either Ly6/G+ or EGFP+ cells present in the spinal cord section.

Digital images were taken at 10×, 20×, 40×, and 60× magnifications using either a Bio-Rad Radiance 2000 MP laser scanning confocal microscope or the Zeiss LSM 510 META-NLO. Images obtained on the Bio-Rad microscope were processed using Laser-Sharp software (Bio-Rad). Alternatively, images were obtained with the Zeiss LSM 510 META-NLO microscope and processed by Zeiss LSM 510 imaging software version 3.0 (Carl Zeiss GmbH, Oberkochen, Germany). Z-stack pictures were taken sequentially every 1.5 μm through the entire tissue section. In addition, some digital images were obtained with an Olympus IX50 epifluorescence microscope and 3CCD Color Digital Video Camera (Olympus Canada Inc., Markham, Canada) using ImagePro 5.1 software and processed using Adobe Photoshop 5.02.

Biochemical Assays

At 24 hours, 72 hours, 1 week, or 2 weeks after injury, mice were anesthetized and perfused with cold 0.9% NaCl. A 0.5-cm-segment of spinal cord centered on the lesion site was removed for analyses. Myeloperoxidase activity was determined as previously described (37). Free radical–induced lipid peroxidation and enzymatic lipid peroxidation, a byproduct of arachidonic acid metabolism, was detected by a thiobarbituric acid–reactive substances assay that measures the relative levels of malondialdehyde (MDA) and other aldehydes as previously described (37).

Production of Bone Marrow Chimeric Mice

Bone marrow was prepared from male C57BL/6 and *lys*-EGFP-*ki* donor animals that were 8 to 10 weeks old (20–30 g), as described (38). After preparation, bone marrow cells were suspended in PBS plus 3% fetal calf serum to a final concentration of 2.5×10^7 cells/mL. Female C57BL/6 and *lys*-EGFP-*ki* recipients (20–30 g) were sublethally irradiated with 899 rad for 8 minutes in a small animal γ-cell irradiation chamber. The bone marrow cell suspension was transplanted into the appropriate recipient 6 hours after irradiation by injecting 5×10^6 whole bone marrow cells into the tail vein. Bone marrow–transplanted mice were allowed to recover for 6 weeks before being subjected to SCI.

Peripheral Blood Preparation for Flow Cytometry

Mice were deeply anesthetized with isoflurane. Blood samples were obtained by intracardiac injection of heparin before cardiac puncture. Red blood cells were lysed by ACK
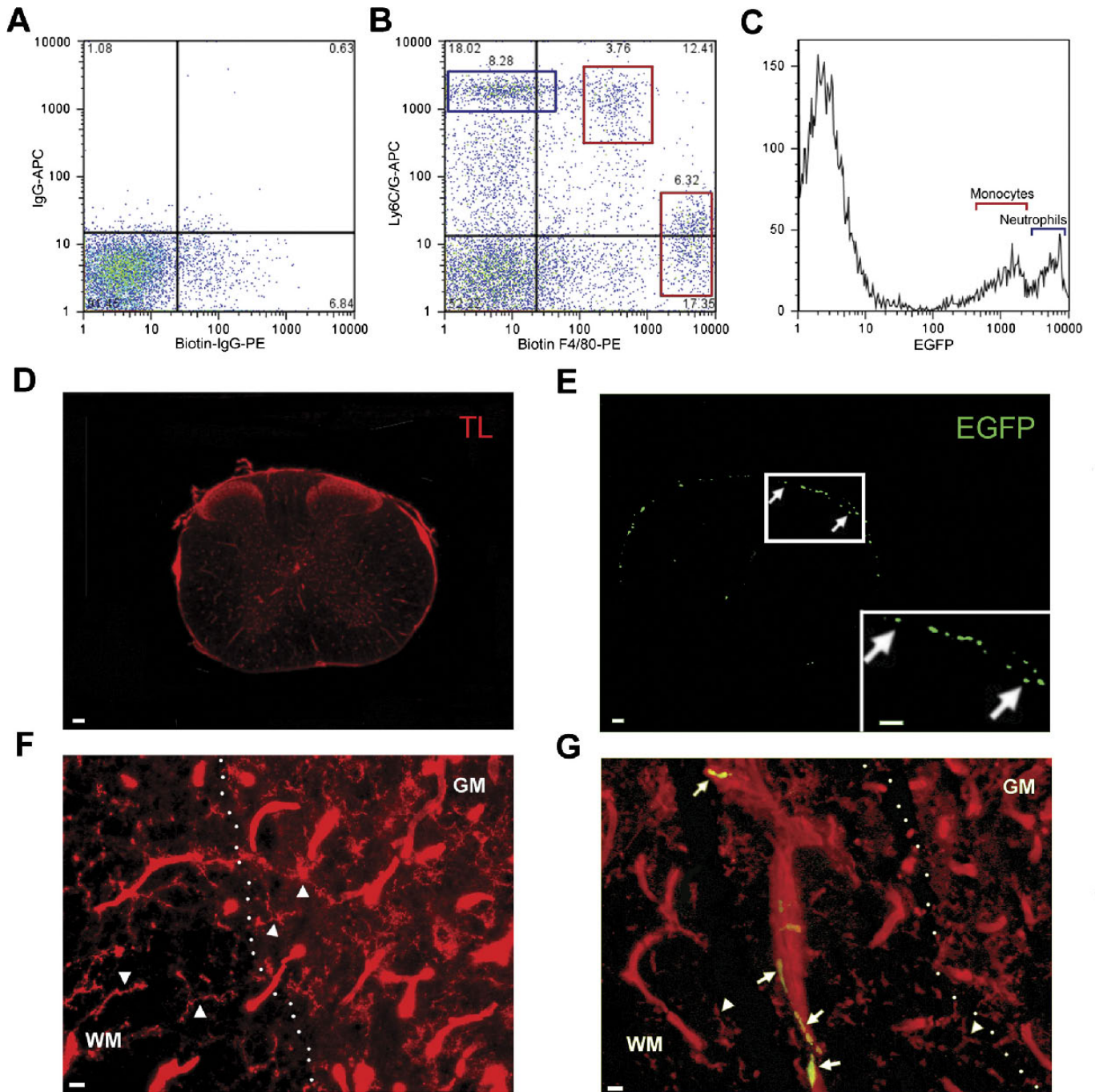
FIGURE 1. Blood profile. **(A)** Isotype controls scatter plot. **(B)** F4/80-Ly6C/G scatter plot of blood showing the neutrophils (F4/80-negative Ly6C/G-positive [blue box]) and the 2 monocyte populations (F4/80-positive Ly6C/G-positive [upper red box] and F4/80-positive Ly6C/G-negative [lower red box]). **(C)** Histogram showing that the neutrophil and the 2 monocyte populations are enhanced green fluorescent protein (EGFP) positive. **(D)** Digital fluorescent images of tomato lectin (TL, red) and anti-EGFP **(E**, green) double-stained normal spinal cord demonstrating EGFP-positive cells in the pia (arrows) but not the cord parenchyma. **(F)** Digital fluorescent images of double stained section showing TL-positive ramified microglia that lack EGFP expression (arrowheads point to microglia). **(G)** Digital fluorescent images of TL-positive, EGFP-positive perivascular cells associated with larger blood vessels (arrows point to EGFP-positive cells). Data are representative of at least 3 independent experiments of 3 or more mice. Scale bars = **(D, E)** 50 μM; **(F, G)** 10 μm.
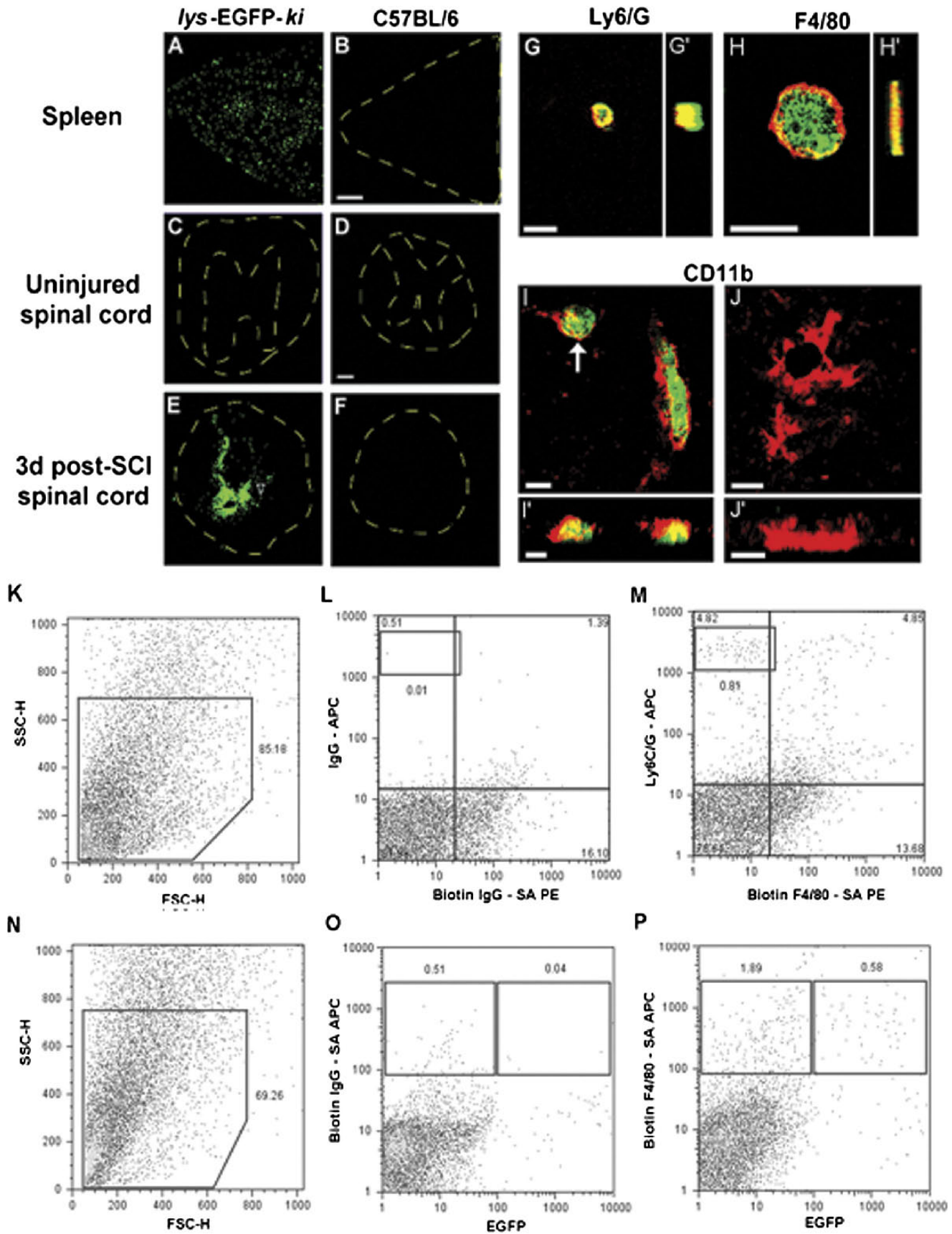
183

TABLE. Comparison of Leukocyte Subsets in Blood, Bone Marrow, and Spleen Between C57BL/6 and *lys*-EGFP-*ki* Mice

	Blood		Bone Marrow		Spleen	
	C57BL/6	*Lys*-EGFP-*ki*	C57BL/6	*Lys*-EGFP-*ki*	C57BL/6	*Lys*-EGFP-*ki*
Classic monocytes Gr-1^{hi}F4/80$^+$	6.2% ± 1.7%	7.8% ± 1.5%	21.7% ± 1.6%	20.1% ± 0.9%	9.3% ± 0.9%	11.5% ± 0.5%
Intermediate subset Gr-1^{int}F4/80$^+$	3.6% ± 0.9%	8.1% ± 1.5%	4.74% ± 1.3%	5.74% ± 1.3%	8.4% ± 0.8%	11.1% ± 1.8%
Nonclassic monocytes Gr-1^{lo}F4/80$^+$	3.7% ± 0.8%	4.1% ± 0.3%	8.73% ± 1.4%	7.43% ± 1.5%	4.0% ± 0.4%	4.3% ± 0.6%
Lymphocytes CD3$^+$CD19$^+$	36.4% ± 0.6%	33.7% ± 2.1%	21.4% ± 2.0%	20.1% ± 1.1%	88.5% ± 1.4%	82.5% ± 5.6%
Neutrophils Gr-1^{hi} Ly6/G^{hi}F4/80$^-$SSC^{hi}	21.9% ± 2.2%	26.3% ± 1.3%	38.8% ± 4.2%	42.4% ± 4.6.%	15.4% ± 0.8%	18.6% ± 3.6%

lysis buffer (Lonza Biowhittaker, Basel, Switzerland). Thereafter, the cells were washed with cold PBS 0.1% BSA and then blocked with 5% (vol/vol) normal goat serum (Jackson ImmunoResearch Laboratories, Inc), followed by a wash with cold PBS 0.1% BSA. Primary antibodies, allophycocyanin-conjugated anti-Ly6C/G (1:400; BD Biosciences, Mississauga, Canada), phycoerythrin-conjugated anti-CD115 (1:100; eBioscience), Alexa Fluor 700–conjugated anti-Ly6/G (1:100; BioLegends, San Diego, CA), and biotinylated anti-F4/80 (1:100; AbD Serotec, Raleigh, NC) were added to 1×10^5 cells per 100 μl in individual flow cytometry tubes (BD Biosciences). For all staining procedures, isotype-matched control antibodies were used. Samples were incubated for 30 minutes on ice in the dark, washed with cold PBS 0.1% BSA, and centrifuged at 6°C. The pelleted cells incubated with biotinylated antibody were resuspended with streptavidin-phycoerythrin or streptavidin-allophycocyanin in PBS 0.1% BSA (1:2000; BD Biosciences) and incubated on ice for 30 minutes in the dark. Finally, cells were washed and resuspended in 400 μl of 0.5% paraformaldehyde fixative.

Spinal Cord Preparation for Flow Cytometry

Transcardiac perfusions were performed with cold Dulbecco modified Eagle medium after SCI. A total of 5 mm of spinal cord was removed (2.5 mm rostral and caudal to the lesion's epicenter at spinal segment T5) from SCI mice (n = 4) and ground between frosted slides into a homogenous cell suspension. The slides were rinsed with cold PBS 0.1% BSA and filtered through a 70-μm strainer. Percoll (Amersham Biosciences, Uppsala, Sweden), made with pH 7.0 to 7.2 via addition of 4-[2-hydroxyethyl]-1-piperazineethanesulfonic acid (Invitrogen Corp, Carlsbad, CA) was added to the cell suspension to make a final concentration of 30% vol/vol and centrifuged on a Percoll gradient to enrich for microglia/mMΦ and hematogenous leukocytes (39). The banded cells were removed from the gradient, washed, and labeled with antibodies as described previously for blood leukocytes.

Flow Cytometry

Blood and spinal cord cells were collected on a BD Biosciences fluorescence-activated cell sorting Calibur analog cytometer. Data acquisition was done using CELLQuest software (version 10; BD Biosciences, Franklin Lakes, NJ). Analysis was performed on FlowJo software version 7.1.2 (Tree Star, Inc, Ashland, OR). The viability of blood and spinal cord samples was determined using the viability marker 7-aminoactinomycin D.

Statistics

All experimental groups of mice contained 3 to 5 mice. Data are expressed as mean ± SEM. Graphic displays and Student *t* test were performed using GraphPad Prism (version 4.0; GraphPad Software, La Jolla, CA). Two-way and one-way analyses of variance were done using GB Stat (version 7; Dynamic Microsystems, Inc, Silver Spring, MD) or Sigma

FIGURE 2. Enhanced green fluorescent protein (EGFP) expression in spinal cord injured *lys*-EGFP-*ki* mice. **(A–F)** Hatched yellow lines demarcate the outer edge of the spleen, spinal cord, and the gray matter and white matter interface. Fluorescent images of uninjured *lys*-EGFP-*ki* **(A)** C57BL/6 **(B)** mice show EGFP expression only in the *lys*-EGFP-*ki* mouse spleen. Uninjured spinal cord sections of *lys*-EGFP-*ki* **(C)** and C57BL/6 **(D)** mice lack significant EGFP (green) expression (pia removed from the spinal cord before sectioning). *Lys*-EGFP-*ki* T4 spinal cord section at 3 days after SCI shows extensive EGFP expression **(E)** (open arrow head indicates an EGFP-positive cell). No EGFP expression is observed in an equivalently injured C57BL/6 mouse T4 spinal cord section **(F)**. **(G–J)** Alternate *lys*-EGFP-*ki* T4 spinal cord sections 3 days after SCI labeled with anti-Ly6/G **(G)**, anti-F4/80 **(H)**, and anti-CD11b **(I)** antibodies. Digital confocal images were taken at the lesion site along with corresponding Z-stacked images **(G′, H′, I′, J′)** taken every 1.5 μm and viewed perpendicularly. Anti–Ly6/G-positive (red) stained EGFP-positive (green) neutrophil **(G′)**. Anti-F4/80 (red) stained EGFP-positive (green) hematogenous monocytes (hMΦ) **(H′)**. Anti–CD11b-positive (red) stained EGFP-positive (green) monocyte-derived microglia (hMΦ) **(I′, arrow)**. An anti-CD11b (red) stained EGFP-negative ramified microglia cell **(J′)**. **(K–P)** Spinal cord forward scatter (FSC) versus side scatter (SSC) profile **(K, N)** was gated to capture single viable cells and then further analyzed with isotype control antibodies to establish positive gates **(L, O)** for F4/80-negative, Ly6/G-positive neutrophils **(M)** and EGFP-negative, F4/80-positive macrophages derived from microglia (mMΦ) and EGFP-positive, F4/80-positive hMΦ **(P)**. Scale bars = **(B, D)** 200 μm and applies to **A, C, E,** and **F; (G, H)** 10 μm; **(I, I′, J, J′)** 5 μm.

Stat (version 3.0; Systat Software, Inc, San Jose, CA) followed by a Student-Newman-Keuls test for post hoc analysis. For analysis, statistical significance was accepted at p ≤ 0.05.

RESULTS

Microglia Lack EGFP Expression in Normal *lys*-EGFP-*ki* Mice

We examined the expression of EGFP in myeloid cells of the blood and in the spinal cord of normal and SCI adult homozygous *lys*-EGFP-*ki* mice. Flow cytometry of blood samples demonstrated EGFP-positive, Ly6C/G-positive, F4/80-negative neutrophils, and EGFP-positive expression in the 2 major monocyte populations (EGFP-positive, Ly6C/G-positive, F4/80^{low} classic or proinflammatory monocytes and the EGFP-positive, Ly6C/G-negative, F4/80^{high} nonclassical monocytes) (Figs. 1A–C). These are the 2 best-described populations of monocytes known to circulate in the blood of the mouse (35, 40, 41); these data confirm that the mice expressed the transgene in the correct population of leukocytes. In contrast, the uninjured spinal cord of the *lys*-EGFP-*ki* mice was largely devoid of EGFP expression throughout the gray and white matter (Figs. 1D–G). Enhanced green fluorescent protein–positive monocyte/macrophages positive for TL staining (Figs. 1D, E) as well as F4/80 (data not shown) were observed throughout the pia that surrounds the spinal cord. Tomato lectin–positive microglia exhibiting a typical ramified morphology were uniformly negative for EGFP expression (Figs. 1F, G). Occasionally, EGFP-positive leukocytes were observed in association with some, but not all, blood vessels. Their spindle-shaped morphology suggested they were likely perivascular macrophages (Fig. 1G) (42, 43). Similar results were observed in normal *lys*-EGFP-*ki* brains and in brains of *lys*-EGFP-*ki* mice subjected to LPS-induced systemic inflammation (Figure, Supplemental Digital Content 1, http://links.lww.com/NEN/A310). Taken together, these results indicate that microglia in the normal and inflamed CNS do not seem to express detectable levels of EGFP. However, in normal *Lys*-EGFP-*ki* mice, but not in wild-type C57BL/6 mice, the spleen (Figs. 2A, B), as well as the bone marrow, lungs, and liver, and lymph nodes (as determined by fluorescence microscopy and/or flow cytometry; data not shown) all contained EGFP-positive cells of the myeloid lineage and/or tissue macrophages. Flow cytometric analysis of the blood, bone marrow, and spleen (independent of EGFP expression) demonstrated no significant differences in the percentage of monocyte subsets, lymphocytes, and neutrophils between wild-type C57BL/6 mice and *lys*-EGFP-*ki* mice (Table).

Microglia Lack EGFP Expression in SCI *lys*-EGFP-*ki* Mice

We next examined EGFP expression in the injured spinal cord of *lys*-EGFP-*ki* mice. Very little EGFP-positive fluorescence was observed in the uninjured spinal cord at T5, and none was observed in a comparable region of spinal cord from a wild-type C57BL/6 mouse (Figs. 2C, D). At 3 days after injury at T5, green fluorescence derived directly from EGFP was present in the lesion (Fig. 2E), but not in the T5

lesion of a wild-type C57BL/6 mouse (Fig. 2F). To identify the EGFP-positive cells, fixed cryosections were immunostained (without detergent to avoid quenching EGFP-derived fluorescence) with antibodies to cell surface markers expressed by neutrophils and microglia, mMΦ and hMΦ. Anti-Ly6/G is a marker found predominantly on neutrophils (Figs. 2G, G'). The presence of side scatter^{hi} (SSC^{hi}) Ly6C/G-positive, F4/80-negative neutrophils in the 3-day injured spinal cord was confirmed by flow cytometry (Figs. 2K–M). Subsequent backgating on the SSC^{hi} Ly6C/G-positive, F4/80-negative population demonstrated that they were EGFP positive (data not shown). Enhanced green fluorescent protein–positive, F4/80-positive (Figs. 2H, H') and EGFP-positive, CD11b-positive (Figs. 2I, I') hMΦ were detected in the lesion 3 days after SCI by immunohistochemistry and at 7 days after SCI by flow cytometry (Figs. 2N–P). Enhanced green fluorescent protein–negative, CD11b-positive mMΦ were detected by immunohistochemistry in the lesion 3 days after SCI (Figs. 2J, J'), and EGFP-negative, F4/80-positive mMΦ were detected by flow cytometry 7 days after SCI (Figs. 2N–P). These results support the hypothesis that microglia and mMΦ can be distinguished from hMΦ expressing EGFP in the *lys*-EGFP-*ki* transgenic mouse SCI model.

To verify that microglia and mMΦ lack EGFP expression, we performed 2 additional experiments, one involving reciprocal bone marrow transplantation between *lys*-EGFP-*ki* and C57BL/6 mice and one involving depletion of hematogenous monocytes using clodronic acid liposomes (Fig. 3). We transplanted bone marrow obtained from *lys*-EGFP-*ki* mice into recipient C57BL/6 mice with the expectation that, after SCI, the ensuing cellular inflammatory response would look phenotypically similar to that seen in *lys*-EGFP-*ki* mice because the only hematopoietic cells expressing EGFP would be of donor origin, whereas microglia and mMΦ could not express EGFP because they lack the transgene (Figs. 3A, B). Using a reverse experimental design, bone marrow from C57BL/6 mice was transplanted into *lys*-EGFP-*ki* mice. In this situation, the only hematopoietic cells that could potentially express EGFP would be the microglia and mMΦ present in the recipient *lys*-EGFP-*ki* mice because the circulating leukocytes would lack the EGFP transgene. Immediately, before SCI, recipient blood samples were analyzed for EGFP expression. Less than 4% of the circulating blood leukocytes expressed EGFP compared with normal *lys*-EGFP-*ki* mice (~27%). Enhanced green fluorescent protein–positive, TL-positive cells were almost completely absent from the lesion at 7 days after injury (Fig. 3C). Quantification of sections from these same mice double stained for F4/80 and EGFP revealed extensive F4/80 immunoreactivity and very little EGFP immunoreactivity throughout the lesion area (Fig. 3D).

Clodronate liposomes have been frequently used to deplete monocyte populations (3, 44–46). Initially, we performed a control experiment to demonstrate that clodronate liposomes did not enter the SCI lesion. To do this, control liposomes containing only PBS were labeled with the membrane-intercalating dye PKH26 (red) and injected i.v. (via the tail vein) and i.p. either once, 1 day before SCI, or twice, 1 day before SCI and at Day 3 after SCI. Neither at Day 1 nor at Day 4 after SCI could PKH26-positive liposome material be detected in the T5
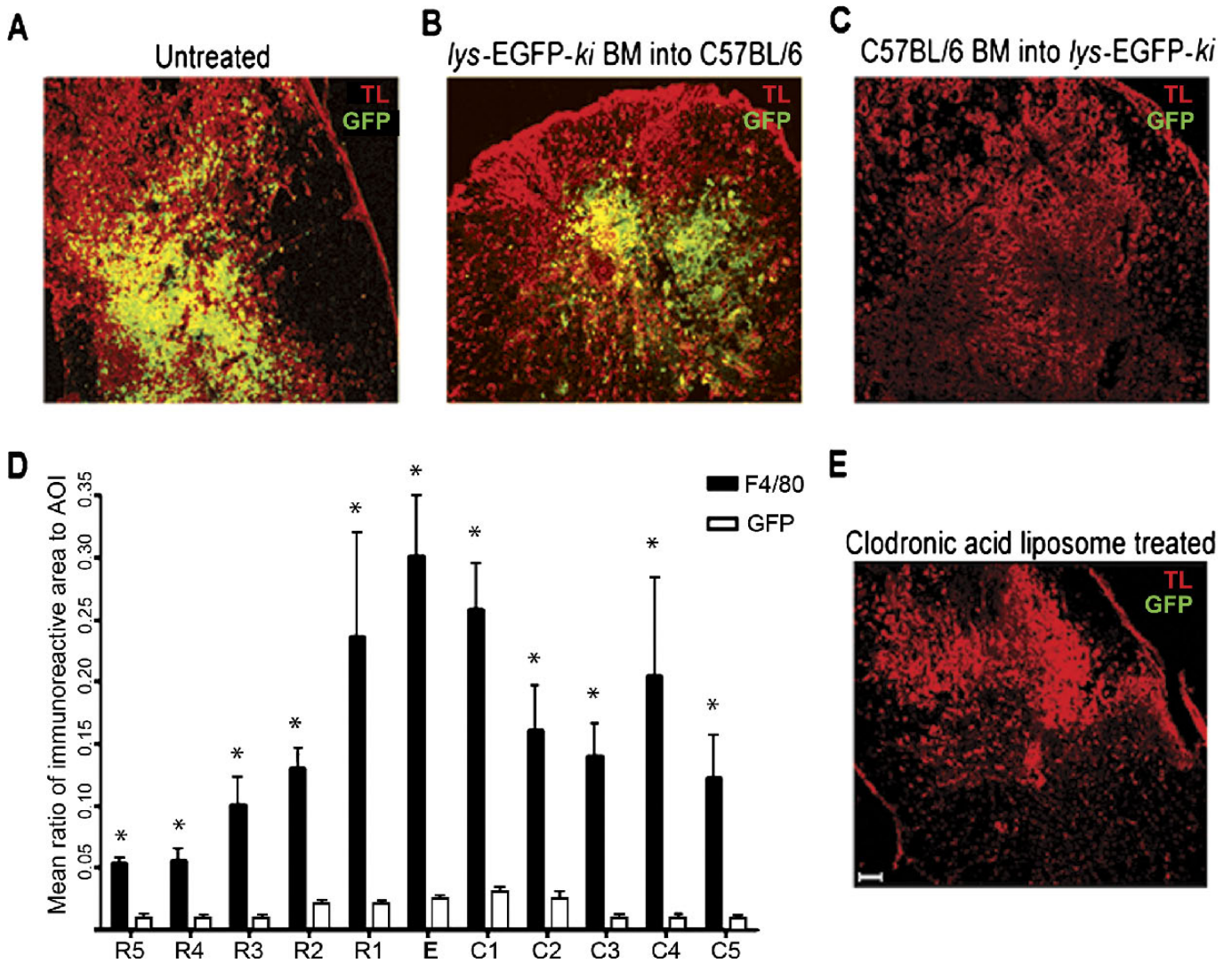
FIGURE 3. Reciprocal bone marrow (BM) transplantation and clodronic acid liposome depletion studies demonstrating a lack of enhanced green fluorescent protein (EGFP) expression in microglia-derived macrophages (mMΦ) at 7 days after spinal cord injury (SCI). **(A, B)** Digital fluorescence images show that the distribution of EGFP-positive (green) and tomato lectin (TL)–positive (red) hematogenous monocytes (hMΦ) in the spinal lesion of a *lys*-EGFP-*ki* SCI mouse **(A)** is the same as in a wild-type C57BL/6 mouse **(B)** transplanted with BM from *lys*-EGFP-*ki* mice (n = 4). **(C)** In the reciprocal situation, where *lys*-EGFP-*ki* mice were transplanted with wild-type C57BL/6, BM EGFP-positive (green) TL-positive (red) monocyte-derived microglia (hMΦ) are absent from the lesion (n = 4). **(D)** Alternate sections of the lesions of mice described in C were stained for EGFP and F4/80 (R is rostral, E is epicenter, C is caudal). Quantitative analysis revealed that F4/80-positive cells are abundantly present and distributed throughout the lesion; EGFP expression is absent. Significant differences between F4/80 and EGFP expression were assessed using a one-way analysis of variance followed by a Student-Newman-Keuls post hoc test (p < 0.05) and indicated with asterisks. **(E)** A clodronic acid liposome-treated SCI *lys*-EGFP-*ki* mouse also shows lack of EGFP expression in TL-positive mMΦ (n = 4). Scale bars = **(E)** 20 μm and applies to **A** to **C**.

spinal lesion, but it was readily detected in the spleen (Figure, Supplemental Digital Content 2, http://links.lww.com/NEN/A311). In addition, after clodronic acid liposome treatment, flow cytometry was performed for each treated animal on the splenocytes and peripheral blood leukocytes to confirm depletion of F4/80-positive blood monocytes. Only animals that were determined to be depleted (having <10% of the normal number of EGFP-positive leukocytes) were used in the study (data not shown). We also determined that significant numbers (>10%–15%) of EGFP-positive, F4/80-positive blood

monocytes did not reappear in the blood until 3 to 4 days after depletion, consistent with previous reports (47). Thus, we treated SCI mice every fourth day with clodronic acid liposomes during a period of 14 days. This led to the successful depletion of EGFP-positive monocytes resulting in the absence of EGFP-positive hMΦ in the injured spinal cord (Fig. 3E). Thus, the BM transplant data and the monocyte depletion data together indicate that the activation and differentiation of microglia into mMΦ does not lead to significant EGFP expression.
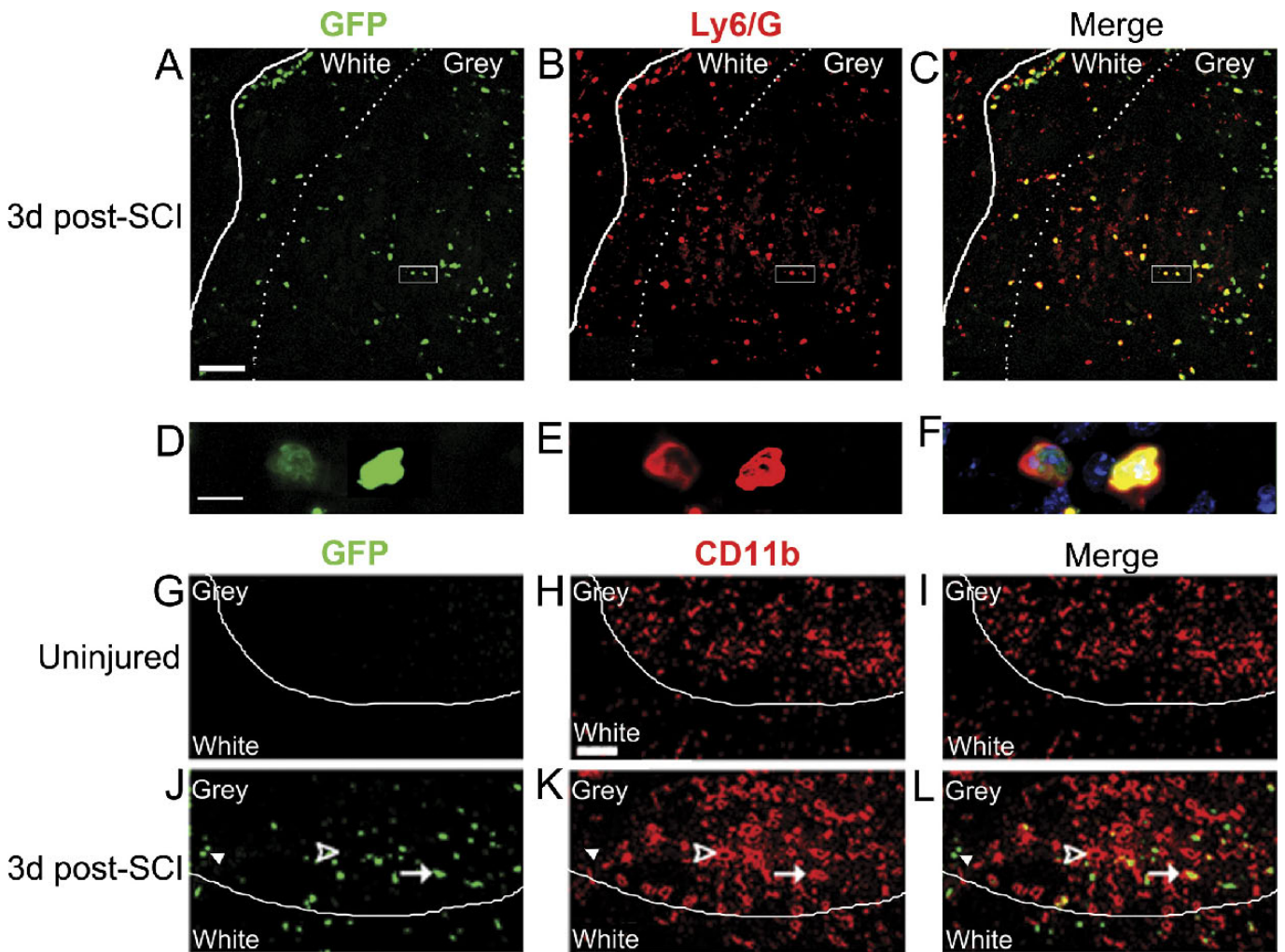
187

© 2012 American Association of Neuropathologists, Inc.
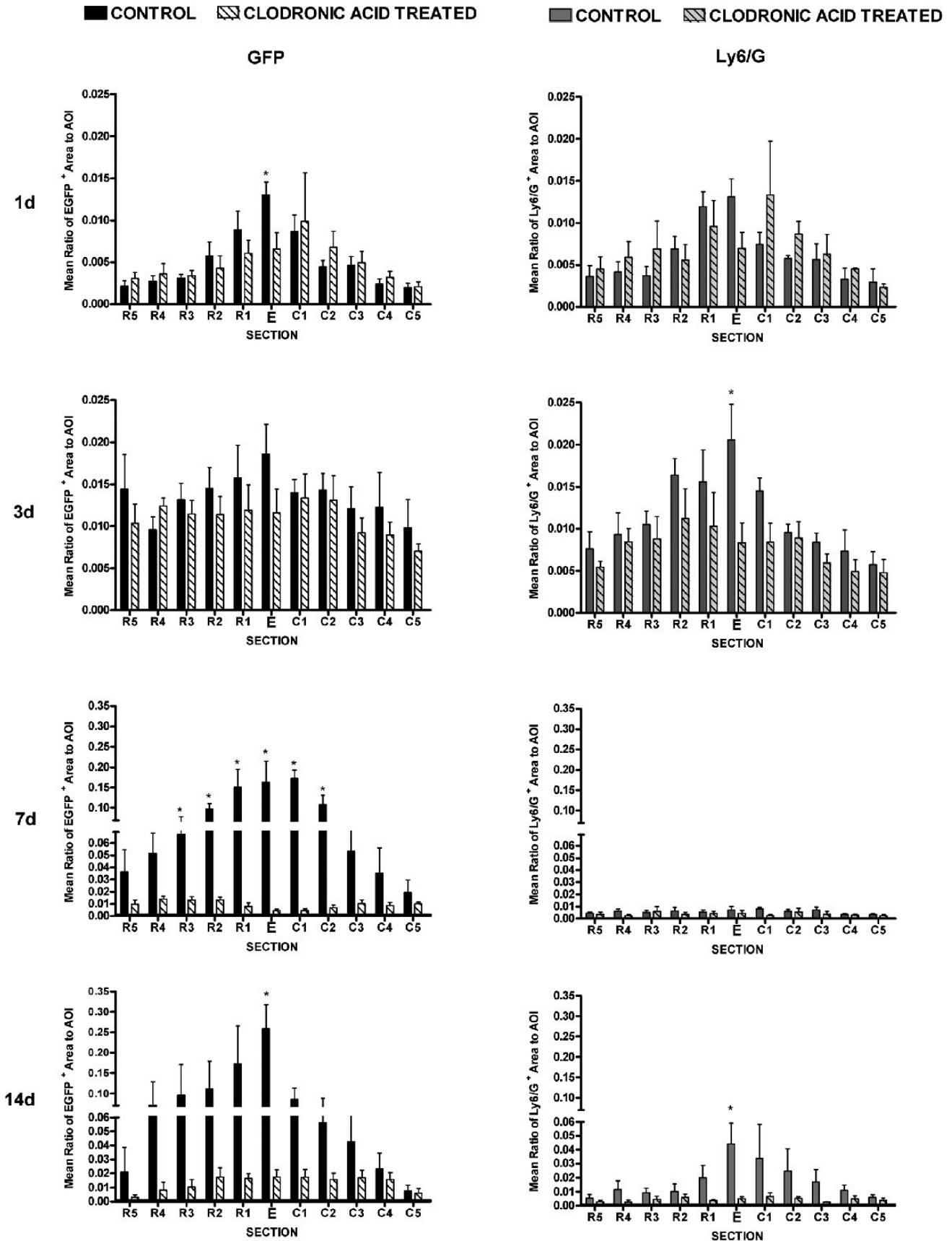
FIGURE 5. Distribution of neutrophils and macrophages in *lys*-EGFP-*ki* mice at 3 days after spinal cord injury (SCI). **(A–F)** Confocal images of spinal cord lesion sections from *Lys*-EGFP-*ki* mice (n = 4) 3 days after SCI stained with anti-green fluorescent protein (GFP) **(**green; **A, D)** and anti-Ly6/G (red; **B, E)** and then merged **(C, F)**. Boxed areas in **A** to **C** are enlarged with nuclear 4′,6-diamidino-2-phenylindole staining (blue) in **D** to **F**. **(G–L)** Confocal images of anti-GFP- **(**green; **G, J)** and anti-CD11b- **(**red; **H, K)** stained spinal cord sections from an uninjured spinal cord **(G–I)** and at the lesion 3 days after SCI **(J–L)** followed by a merged image **(I, L)**. An example **(J–L)** of a CD11b-positive, EGFP-negative activated macrophage derived from microglia (mMΦ) is indicated by an open arrowhead; a CD11b-positive, EGFP-positive hematogenous monocyte (hMΦ) is indicated by an arrow. EGFP-positive, CD11b-negative neutrophils are indicated by closed arrowhead. Scale bars = **(A)** 100 μm applies to **B** and **C**; **(D)** 10 μm and applies to **E** and **F**; **(G)** 50 μm and applies to **H** to **L**.

Expression and Distribution of EGFP-Positive Neutrophils and hMΦ in the Injured Spinal Cord: Days 1 and 3

A digital morphometric assessment was performed to determine the distribution of EGFP-positive cells in the SCI lesion. Because microglia and mMΦ lack EGFP expression, such an assessment would not be confounded by phenotypic markers that failed to discriminate between hematogenous leukocytes and microglia and mMΦ. Enhanced green fluorescent protein–positive neutrophils were identified by staining with anti-Ly6/G antibody (an antibody that binds to neutrophils but not monocyte/MΦ) and by their resistance to clodronic

FIGURE 4. Quantification of Ly6/G and enhanced green fluorescent protein (EGFP) expression in control and clodronic acid liposome-depleted animals at 1, 3, 7, and 14 days after spinal cord injury (SCI). The mean ratio of EGFP-positive area or Ly6/G-positive area to area of interest (cross section of the spinal cord) is displayed in relation to the injured spinal cord section on the x axis (R is rostral, E is epicenter, C is caudal). Variability is indicated by standard error bars for each group (n = 4). Significant differences between the control and clodronic acid treated animals were assessed using a one-way analysis of variance followed by a Student-Newman-Keuls post hoc test (p < 0.05) and indicated with asterisks.
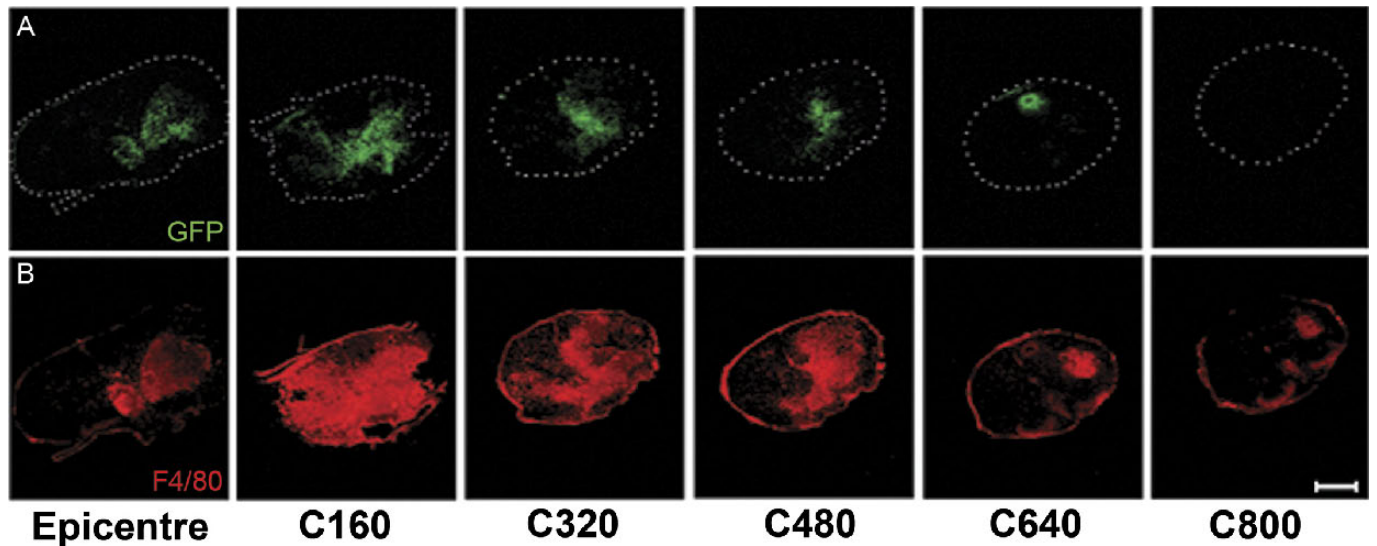
© *2012 American Association of Neuropathologists, Inc.*
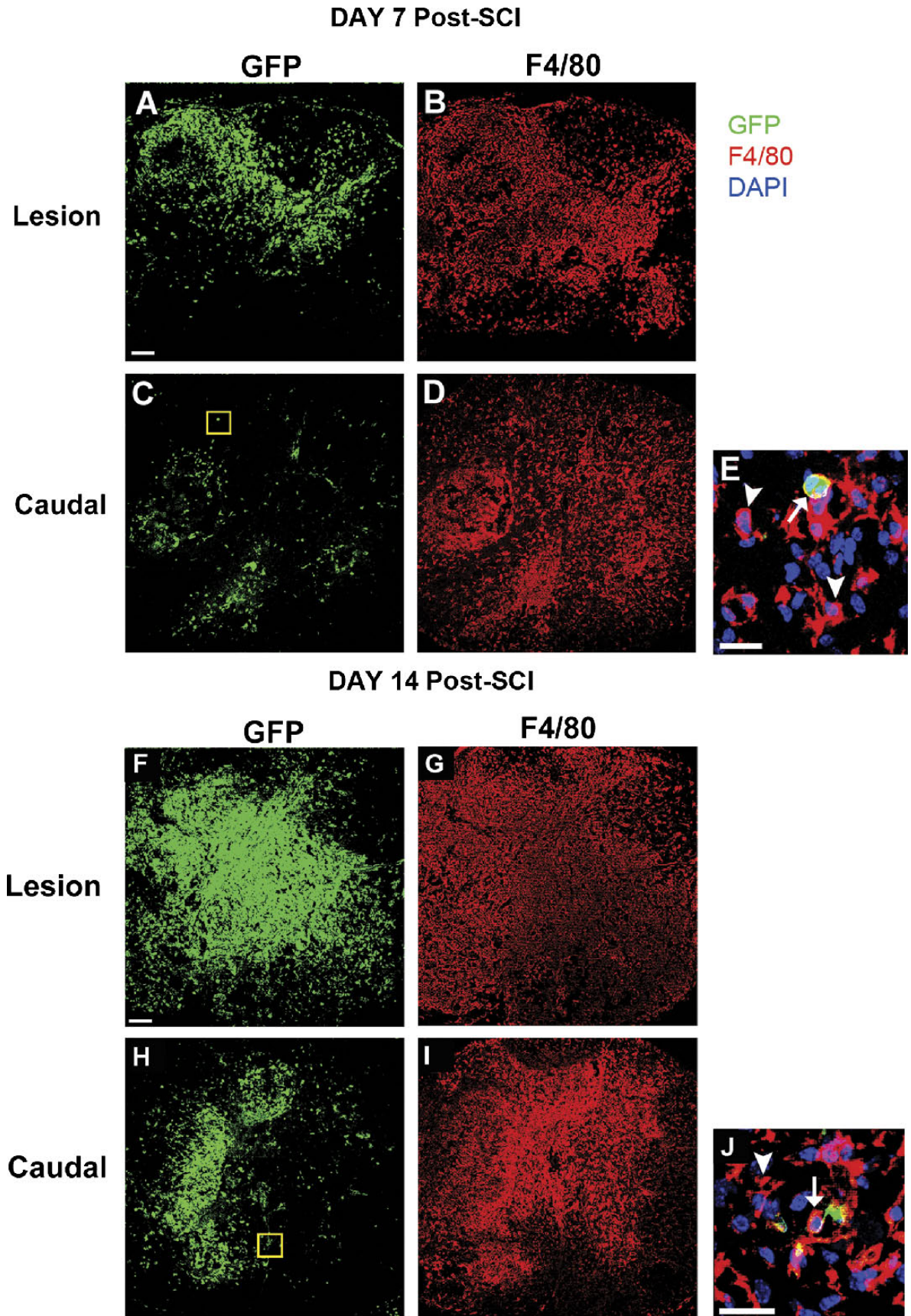
FIGURE 7. Clusters of enhanced green fluorescent protein (EGFP)–negative, F4/80-positive microglia macrophages (mMΦ) extend beyond the presence of EGFP-positive hematogenous macrophages (hMΦ) in untreated *lys*-EGFP-*ki* mice at 14 days after spinal cord injury (SCI). Spinal cord sections (dorsal side of cord is at the top of each image) from SCI mice were double stained with anti-GFP **(A**, green) and F4/80 **(B**, red) antibodies. The numbers below panel **(B)** indicate the distance (in μm) each section is from the section shown in the epicenter of the lesion in the caudal [C] direction. The distributions of EGFP-positive and F4/80-positive cells were examined at the epicenter and in sections caudal to the lesion site at 160-μm intervals. Clustered EGFP-negative, F4/80-positive microglia extend beyond the point at which EGFP-positive, F4/80-positive hMΦ can last be observed at 640 μm caudal to the lesion. Scale bars = 300 μm.

acid liposome treatment, which allowed them to be distinguished from clodronic acid liposome treatment-sensitive EGFP-positive Ly6/G-monocyte/hMΦ. Flow cytometry performed on the blood of each mouse at the time of death revealed that the percentage of GFP-positive neutrophils (∼60%–70% of all EGFP-positive blood leukocytes) did not vary substantially during the 14-day time course of clodronate liposome treatment. All mice responded to the clodronate treatment.

At 8 hours after SCI, the infiltration of Ly6/G-positive and EGFP-positive leukocytes was not significant (data not shown). The level of EGFP and Ly6/G expression increased starting on Day 1 after SCI (Fig. 4). Similar levels of EGFP and Ly6/G expression were also observed at Day 3 (Fig. 4). The EGFP expression was greatest at the lesion's epicenter (E) and decreased steadily in the rostral (R) and caudal (C) sections examined. At both time points, most of the EGFP-positive and Ly6/G-positive cells were resistant to the clodronate liposome treatment, suggesting that they were likely

neutrophils. This result was further confirmed by staining sections for MPO, a known marker of neutrophils (34, 48). The distribution of MPO-positive neutrophils from *lys*-EGFP-*ki* mice across the spinal lesion was similar to the distribution of Ly6/G-positive cells at Day 3 after SCI and was not substantially different from the distribution of MPO-positive cells observed across the lesion of wild-type C57BL/6 mice at Day 3 after SCI (Figure, Supplemental Digital Content 3, http://links.lww.com/NEN/A312). Furthermore, at 1 and 3 days after SCI, spinal cord lesion homogenates from *lys*-EGFP-*ki* SCI mice (n = 4–5) were assayed for MPO enzymatic activity and to detect MDA, a product of lipid peroxidation. In *lys*-EGFP-*ki* mice after SCI, the MPO activity (Day 1, 34 ± 13 U/g tissue; Day 3, 31 ± 9.4 U/g tissue) and MDA (Day 1, 581 ± 32 nmol/L per gram of tissue: Day 3, 457 ± 85) assay results were similar to the values in C57BL/6 mice after SCI for MPO activity (Day 1, 45 ± 3 U/g tissue; Day 3, 28 ± 6.4 U/g tissue) and MDA (Day 1, 474 ± 37 nmol/L per gram of tissue;

FIGURE 6. Distribution of macrophages in mice at 7 and 14 days after spinal cord injury (SCI) reveals clusters of centrally located enhanced green fluorescent protein (EGFP)–positive hematogenous macrophages (hMΦ) surrounded by EGFP-negative microglia and macrophages derived from microglia (mMΦ). **(A–E)** *Lys*-EGFP-*ki* spinal cord sections from mice 7 days after SCI at **(A, B)** and caudal **(**160–320 μm from the epicenter; **C, D)** to the lesion double stained with anti-GFP **(**green; **A, C)** and anti-F4/80 (red; **B, D)**. The yellow box in **C** encloses the area shown with a higher magnification in **E**, a merge of EGFP (green), F4/80 (red), and 4′,6-diamidino-2-phenylindole (blue, for nuclei) staining. Arrow indicates an EGFP-positive, F4/80-positive rounded hMΦ; the arrowhead indicates an EGFP-negative, F4/80-positive ramified mMΦ. **F–J**: *lys*-EGFP-*ki* spinal cord sections from mice 14 days after SCI at **(F, G)** and caudal **(**160–320 μm from the epicenter; **H, I)** to the lesion double stained with anti-GFP **(**green; **F, H)** and anti-F4/80 (red; **G, I)**. The yellow box in **H** encloses the area shown with a higher magnification in **J**, a merge of EGFP (green), F4/80 (red), and 4′,6-diamidino-2-phenylindole (blue, for nuclei) staining. Arrow indicates an EGFP-positive, F4/80-positive rounded hMΦ; the arrowhead indicates an EGFP-negative, F4/80-positive ramified mMΦ. Scale bars = **(A)** 50 μm and applies to **B** to **D** and **F** to **I**; **(E)** 20 μm.

© 2012 American Association of Neuropathologists, Inc.
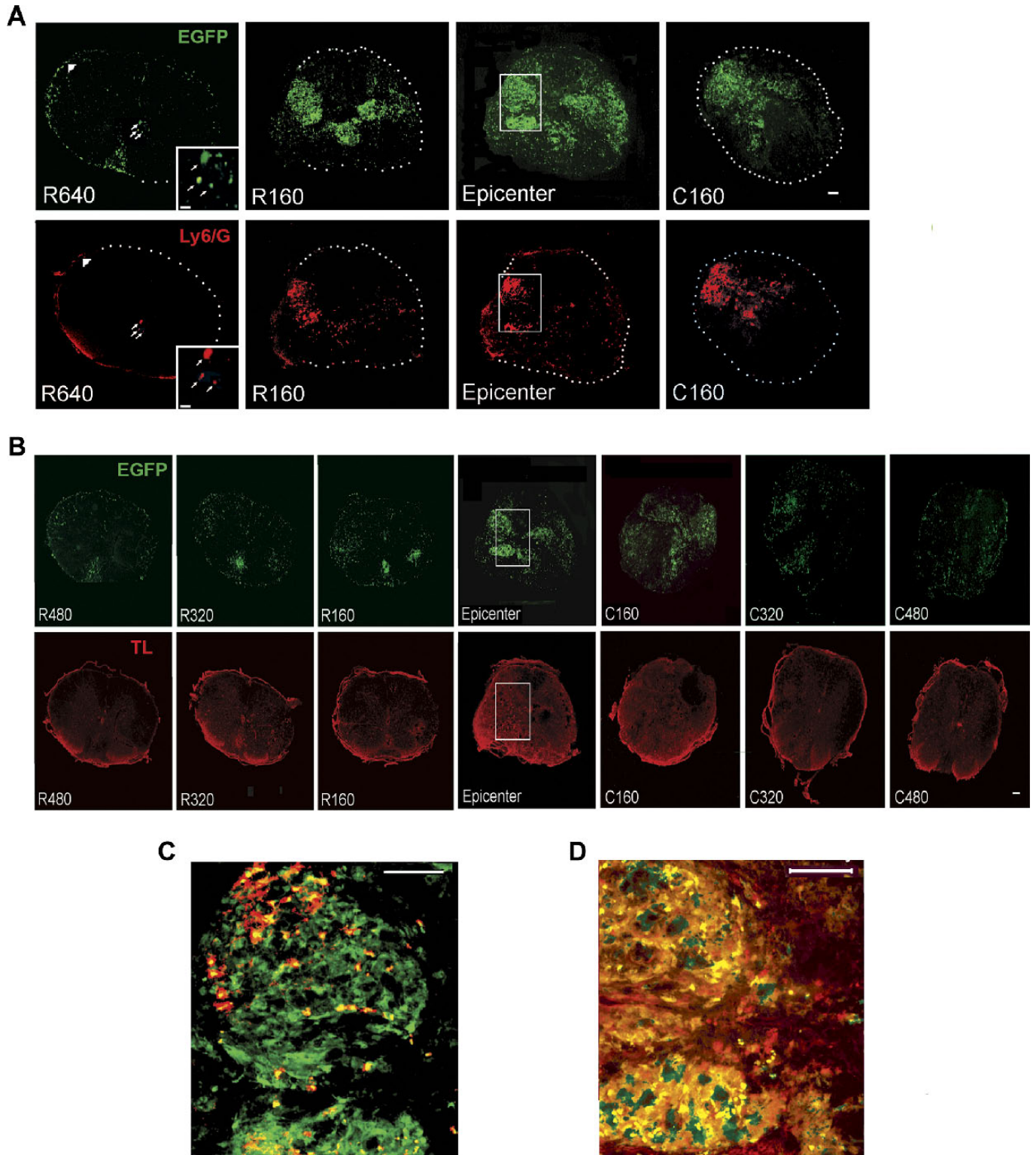
Day 3, 500 ± 34 nmol/L per gram of tissue). These findings indicate that some of the downstream effects of neutrophil and monocyte infiltration within the lesion of *lys-EGFP-ki* mice are not different from those in wild-type C57BL/6 mice.

The spatial distributions of Ly6/G-positive, EGFP-positive and Ly6/G-negative, EGFP-positive cells in the lesion at Days 1 and 3 after SCI were similar, with both cell populations dispersed across the lesion (Figs. 5A–C) and no real concentration in the gray or white matter. To look more specifically at hMΦ and microglia/mMΦ, alternate sections were stained with anti-CD11b because neutrophils rapidly lose CD11b expression after extravasation across the endothelium (49). Like Ly6/G-positive neutrophils, the CD11b-positive, EGFP-positive cells (Figs. 5J–L, arrow) were dispersed throughout the lesion but were more prominent in the gray matter and were surrounded by CD11b-positive, EGFP-negative activated microglia/mMΦ (Figs. 5J–L, open arrowhead). Smaller CD11b-EGFP-positive cells, likely neutrophils, were also present (Figs. 5J–L, closed arrowhead).

Expression and Distribution of EGFP-Positive Neutrophils and hMΦ in the Injured Spinal Cord: Days 7 and 14

At 7 and 14 days after SCI, EGFP expression differed significantly between the untreated control and clodronic acid liposome–depleted groups (Fig. 4). The expression of EGFP in the SCI lesion's epicenter in the untreated control group increased from Day 3 after SCI values by ~8-fold at Day 7 and 14-fold at Day 14. These findings contrasted with the clodronic acid liposome-treated groups in the Days 7 and 14 groups, where EGFP expression decreased almost 36- and 15-fold, respectively, compared with their corresponding untreated groups. On Day 14 after SCI, Ly6/G-positive cells reappeared at the lesion's epicenter (Fig. 4; 14 days) and in the closest adjacent rostral and caudal section. This reappearance of Ly6/G-positive cells, likely neutrophils, seems to depend on the presence of hMΦ as Ly6/G expression did not increase in the lesions epicenters of clodronic acid liposome–treated SCI mice.

The distribution of lesion-associated hMΦ and microglia/mMΦ was characterized at Days 7 and 14 after SCI. Macrophages derived from hematogenous monocytes or microglia were identified by staining with the antibody to the macrophage marker F4/80. At Day 7 (Figs. 6A–E) and Day 14 (Figs. 6F–J), F4/80-positive cells were present. However, rather than being diffusely distributed throughout the lesion, as observed at Days 1 and 3 after SCI, the F4/80-positive macrophages had coalesced more densely. Both individual and

clustered EGFP-positive, F480-positive hMΦ seemed to be surrounded and mixed in with EGFP-negative, F4/80-positive mMΦ (Figs. 6A, B, F, G) at the epicenter, as well caudal (Figs. 6C, D, H, I) and rostral (data not shown) to the epicenter. The morphology of the F4/80-positive, EGFP-positive cells observed at both time points was typical of rounded hMΦ (Figs. 6E, J, arrow). The EGFP-negative, F4/80-positive microglia/mMΦ exhibited either a stellate- or a stubby-activated morphology, particularly near the peripheral edges where macrophages had coalesced or had typical rounded macrophage morphology (Figs. 6E, J, arrowhead). The F4/80-positive, EGFP-positive cells present at Days 7 and 14 after SCI seemed to be concentrated in the regions that normally contain gray matter. In clodronic acid liposome–treated animals, whereas EGFP expression was largely absent (Figure, Supplemental Digital Content 4, parts A, C, E, F, http://links.lww.com/NEN/A314), a condensed but evenly distributed EGFP-negative, F4/80-positive population was still present in the lesion at Days 7 and 14 after SCI, equivalent to that seen in animals that had not been treated with clodronate liposomes.

Examination of the distribution of EGFP-positive and F480-positive cells along the length of the lesion revealed a further difference in the distribution of hMΦ and mMΦ. As shown in Figures 7A and B, clusters of EGFP-negative, F4/80-positive cells persisted for at least 200 to 300 μm beyond the point where EGFP-positive cells could be observed. This was true in the rostral direction as well (data not shown). Thus, the extent of the microglial-based inflammatory response throughout the lesion did not seem to depend on the presence of infiltrating hMΦ. The extent of the spinal lesion (800–1000 μm in length), as assessed by solochrome cyanin staining for myelin was not different from the extent we reported for C57BL/6 mice after clip compression SCI (50).

EGFP Expression in the Injured Spinal Cord at Day 42

At 42 days after injury, we examined sections of injured spinal cord for the presence of neutrophils using the anti-Ly6/G antibody. Enhanced green fluorescent protein–positive, Ly6/G-positive cells were still present but were predominantly restricted to a very narrow region surrounding the epicenter (160 μm on either side; Fig. 8A). At the epicenter, EGFP-positive, Ly6/G-positive cells were distributed throughout but were also interspersed within large clusters of EGFP-positive cells (Figs. 8A, C). Most of the EGFP-positive cells in such clusters were likely hMΦ because an adjacent section stained for TL and EGFP revealed that most cells in the clusters

FIGURE 8. Distribution of anti-Ly6/G and biotinylated tomato lectin (TL) binding and enhanced green fluorescent protein (EGFP) expression in the *lys-EGFP-ki* mice at 42 days after spinal cord injury (SCI). **(A, B)** Spinal cord sections (dorsal side of cord is at the top of each image) from SCI mice 42 days after injury double stained with either **(A)** anti-Ly6/G and anti-EGFP or with **(B)** TL and anti-EGFP reveal the chronic persistence of neutrophils in the lesion area and in clusters of macrophages. The numbers below each panel in **A** and **B** indicate the distance (μm) each section is from the section shown in the epicenter of the lesion in the rostral [R] and caudal [C] direction. Arrowhead in R640 of **A** indicates an example of a Ly6/G-positive, GFP-positive neutrophil in the pia. Arrows in R640 **A** correspond to the arrows in the inset and indicate the location of rare EGFP-positive, Ly6/G-positive cells located in the parenchyma away from the lesion's epicenter. **(C, D)** Magnified merged images of the 2 boxed areas in the epicenter **A** and **B**. Scale bars = **(A, B)** 100 μm; **(C, D)** 50 μm. Scale bar in R640 panels of **A** = 10 μm.

stained positive for both (Fig. 8D). Examination of sections more rostral (Fig. 8A; R640) or caudal (data not shown) to the epicenter revealed very few neutrophils that, when present, were generally located in the pia and occasionally in the parenchyma (Fig. 8A, arrows, R640 panel).

At Day 42 after SCI, EGFP-positive, TL-positive (Fig. 8B) and F4/80-positive (data not shown) hMΦ were still present, although the extent of the cellular inflammatory response was considerably diminished. Moving rostrally or caudally away from the lesion's epicenter, small clusters of EGFP-positive, TL-positive cells, as well as a scattering of individual cells, remained evident (Fig. 8B, R160 μm to R480 μm). At 480 μm rostral to the lesion's epicenter, individual EGFP-positive cells were still evident in cord sections with a relatively normal gray and white matter distribution. In the caudal direction similar, although somewhat larger, clusters and individual groupings of cells were evident in sections immediately adjacent to the epicenter. As on the rostral side, by 480 μm caudal to the lesion, only scattered EGFP-positive, TL-positive cells were evident. This distribution of macrophages contrasts with the broader distribution observed at 14 days after SCI (Fig. 7).

DISCUSSION

The *lys*-EGFP-*ki* transgenic mouse model allows EGFP to mark mature hematogenous granulomyelocytic cells including neutrophils, monocytes, and hMΦ (28). The EGFP gene was knocked into the lysozyme M locus resulting in expression driven by the lysozyme M promoter in its native context. Therefore, EGFP expression faithfully identifies the cells that normally express lysozyme M in the absence of any other genetic or immunologic modification of the mouse. This idea has now been used by others to examine the role of neutrophils and monocyte/macrophages in a model of atherosclerosis (27). The data presented in this study support our contention that EGFP expression in the *lys*-EGFP-*ki* mouse permits the distinction of microglia/mMΦ from neutrophils and monocyte/hMΦ. Our study shows that this transgenic mouse is a convenient and valuable tool for examining the distinct roles of microglia/mMΦ, neutrophils, and monocyte/hMΦ in the injured spinal cord. The control of the lysozyme M promoter in the myeloid lineage cells in peripheral circulation and tissues is likely different from that of CNS microglia because they are ontologically distinct cell lineages (51). In uninjured CNS parenchyma, resting microglia of the brain and spinal cord do not express EGFP in the spinal cord or in the brain. This observation parallels the absence of EGFP expression in *lys*-EGFP-*ki* microglia/mMΦ in other mouse models of CNS pathology, such as experimental autoimmune encephalomyelitis (30), and in the brains of *lys*-EGFP-*ki* mice injected systemically with toxic LPS. Consistent with the known pattern of lysozyme M expression in various mouse tissues (27, 53), uninjured *lys*-EGFP-*ki* mice express EGFP in their circulating leukocytes of the myeloid lineage and in tissue macrophages from spleen, as well as the lung and liver (J. Cheung and G. A. Dekaban, unpublished results). In tissues bordering the CNS (e.g. within blood vessel walls), spindle-shaped EGFP-positive, hMΦ with mor-

phology typical of perivascular MΦ have been observed (43, 54, 55). As expected, we observed EGFP-positive hMΦ within the meninges because these cells regularly interchange with circulating monocytes (54–56). Although not exhaustively assessed, we did not see any substantial differences between *lys*-EGFP-*ki* and wild-type C57BL/6 mice in their leukocyte populations and in their leukocyte responses to SCI. Thus, the *lys*-EGFP-*ki* transgenic mouse offers an alternative model to allow hMΦ and mMΦ to be distinguished easily without injuring the animal or perturbing the immune system of the animal before SCI.

Experimental approaches to distinguishing microglia and mMΦ from monocytes and hMΦ include selectively depletion of hematogenous monocytes and hMΦ with the aim of examining only the microglial and mMΦ response (3). However, in the absence of hMΦ, the spatial, temporal, and functional nature of the microglial-based response may be altered. Bone marrow chimeras derived by transplantation of donor cells expressing either a different MHC haplotype or expressing GFP also have been used to identify aspects of the temporal and spatial distribution of hMΦ and mMΦ (16, 18). However, the generation of bone marrow chimera requires that the recipients be lethally irradiated, resulting in injury to the recipient that includes the CNS. Such irradiation-induced CNS injury can result in the arrival of donor bone marrow progenitors into the spinal cord and replacement of endogenous microglia with donor-derived cells that differentiate into microglia of the donor genetic background (24). The degree of chimerism is seldom described nor is the uniformity of chimerism ensured within a group of animals under study. Thus, interpretation of data from analyses of bone marrow chimeras may not always be clear. Shielding the head during radiation or minimizing the dose of radiation needed seems to minimize but may not eliminate this problem (18, 57).

To verify further that microglia and mMΦ did not convert to an EGFP-positive phenotype after SCI, bone marrow transplantation and hematogenous monocyte depletion were carried out. In neither case did microglia become EGFP positive. In the clodronic acid liposome depletion experiments, we injected the liposomes only into the blood and peritoneal cavity to produce an optimal depletion of systemic monocytes and hMΦ. Clodronic acid liposomes administered in this manner do not deplete EGFP-positive neutrophils, perivascular, or meningeal MΦ or EGFP- microglia or mMΦ (58–60). We did not inject the clodronate liposomes into the fourth ventricle, a method known to deplete meningeal and perivascular MΦ (58) because this could have led to depletion of activated microglia and mMΦ in the presence of the SCI. Thus, the EGFP-positive meningeal and perivascular hMΦ both can migrate to sites of CNS inflammation (43, 54, 55) and may have contributed to few the EGFP-positive cells present in the lesion's epicenter and surrounding areas. Because the number of meningeal or perivascular EGFP-positive hMΦ in the injured spinal cord was small, these hMΦ would have contributed only a minor portion of the EGFP-positive hMΦ found at the lesion.

On the basis of the quantitative immunohistochemical and flow cytometry analysis, the temporal appearance and spatial distribution of microglia/mMΦ, neutrophils, and hMΦ

confirm previous data of others using rat and mouse models (1, 16, 56, 60–63). The data also closely parallel the observations obtained from an analysis of human SCI (32). Neutrophils in mice appear in maximal numbers at 3 days after SCI, as shown here and by others (52). This is more similar to human SCI in which we reported peak numbers at Days 3 to 5 after injury (32) as opposed to the rat where peak numbers of neutrophils appear much earlier at 8 hours (34). All 3 species have a similar macrophage response that peaks at 7 days after SCI (33, 52). These similarities validate the present model for study of the cellular inflammatory response to SCI. The similarity of our results with the data gathered using bone marrow transplantation after full body irradiation suggests that radiation-induced CNS injury in mice and rats does not significantly affect the nature of the ensuing inflammatory response after SCI. Furthermore, the data also demonstrate that the cellular inflammatory response in the clip compression injury used in this study is similar to that in contusion injury models used by others (1, 16, 52). Thus, ischemic injury, at least within the time frame of our study, did not induce substantial qualitative differences in the inflammatory response when compared to the contusion injury. This conclusion should be verified directly by a study of contusion SCI in the *lys*-EGFP-*ki* mouse.

Despite the similarities in our data to those of others, there were additional notable findings. Unlike depletion studies in the rat, where macrophages were absent in the central gray matter of the lesion, we found that the mMΦ were distributed throughout the lesion area. Furthermore, in mice that are not depleted, EGFP-positive hMΦ seem to be centrally located and to dominate the macrophage clusters in the lesion; these EGFP-positive hMΦ are interspersed with mMΦ in areas normally containing gray matter. The EGFP-positive hMΦ are surrounded by large numbers of activated stellate microglia and mMΦ. Although this is similar to some reports in mice and rats (16, 52), our data contrast with the observations of Schecter et al (18) in which hMΦ were described as confined to the edges of the lesion without entering it. Our data clearly support the concept that hMΦ infiltrate the center of the lesion and are available to clear cellular debris and participate in other wound healing activities.

The clusters of EGFP-mMΦ that extended beyond the presence of EGFP-positive hMΦ at 14 days after SCI has not been previously demonstrated in mice; this finding is consistent with data obtained in SCI rats (16). By 42 days after SCI, both the hMΦ and the microglial and mMΦ distribution had shortened significantly, and they were concentrated predominantly near the lesion's epicenter. At this chronic time point, the remaining macrophage inflammatory response was focused in smaller clusters of hMΦ interspersed with Ly6/G-positive neutrophils surrounded by a less extensive layer of mMΦ and microglia.

Finally, our data confirm that Ly6/G-positive neutrophils in mice have a peak response at 3 days after SCI but do not completely disappear thereafter. Rather, Ly6/G-positive neutrophils continue to persist at the lesion's epicenter and regions immediately adjacent to the epicenter for at least 6 weeks. This is consistent with the findings of others, as well as our recent findings in C57BL/6 mice (50, 52). Importantly,

because clodronic acid liposome depletion of hMΦ prevented the reappearance of Ly6/G-positive neutrophils from appearing at Day 14, our data indicate that the reappearance of the Ly6/G-positive neutrophils at Day 14 (and likely beyond) may depend on the presence of hMΦ. The arriving hMΦ likely produce a second wave of cytokines (e.g. tumor necrosis factor and macrophage-derived neutrophil chemotactic factor) and chemokines that recruit additional neutrophils to the lesion's epicenter and/or extend the life of neutrophils beyond their typical short life span (64). Further investigation is required to understand the exact mechanism behind the reappearance of the Ly6/G-positive cells. The persistence of neutrophils in mice may contribute to the establishment of a chronic inflammatory state in the SCI lesion area. It is becoming increasingly evident that neutrophils may have more complex role to play in inflammation with possible participation in antigen presentation, autoimmunity, and regulation of T-cell responses (65), but the significance of this observation needs to be considered carefully because a prolonged neutrophil presence has not been observed in other species including humans (33, 66).

Marker expression of EGFP under the control of the lysozyme M promoter should be a useful tool in the presence of microglia and mMΦ to determine whether the various monocyte subsets that exist in the blood have similar counterparts as hMΦ in SCI lesions. Within the blood, at least 2 monocyte subsets (i.e. classic or proinflammatory monocytes [Ly6C/G-negative, F4/80^{low}] and the nonclassic subset [Ly6C/G-negative F4/80^{hi}]) are easily identified; the latter are thought to be the pool of monocytes that maintain populations of tissue macrophage and have a role in tissue homeostasis (35, 40). Others have defined monocyte/macrophages on a more functional basis, such as the M1 and M2 classification, which consists of at least 3 possible M2 subsets (67–69). The M1 and M2 classification seems to relate to the classic and nonclassic definition of monocyte subsets, respectively. M1 and M2 macrophages both exist in the lesion of SCI mice with the presence of M1 macrophages associated with neuronal toxicity (23, 68, 69), although the absolute nature of this conclusion remains in question (18, 57). Using the *lys*-EGFP-*ki* mouse, it will be possible to distinguish M1 and M2 hMΦ from mMΦ, thereby permitting a more accurate assessment of the phenotype and function of these 2 populations. Our study also suggests that the lysozyme M Cre conditional knockout mouse could be very useful in differentially knocking out genes in neutrophils, monocytes, and/or hMΦ whereas not affecting microglia and mMΦ (70, 71). Furthermore, preclinical studies involving therapies to reduce the inflammatory response mediated by hematogenous neutrophils and monocyte/hMΦ will be able to assess the effects of therapy on these EGFP-positive myeloid cells without being confounded by the presence of microglia/mMΦ. Such studies may further define the role of microglia/mMΦ and hMΦ in SCI and lead to improved and more targeted therapies to enhance neuroprotection and neuroregeneration of the injured spinal cord.

REFERENCES

1. Carlson SL, Parrish ME, Springer JE, et al. Acute inflammatory response in spinal cord following impact injury. Exp Neurol 1998;151:77–88
2. Blight AR. Effects of silica on the outcome from experimental spinal cord injury: Implication of macrophages in secondary tissue damage. Neuroscience 1994;60:263–73
3. Popovich PG, Guan Z, Wei P, et al. Depletion of hematogenous macrophages promotes partial hindlimb recovery and neuroanatomical repair after experimental spinal cord injury. Exp Neurol 1999;158:351–65
4. Wells JE, Hurlbert RJ, Fehlings MG, et al. Neuroprotection by minocycline facilitates significant recovery from spinal cord injury in mice. Brain 2003;126:1628–37
5. Chen M, Ona VO, Li M, et al. Minocycline inhibits caspase-1 and caspase-3 expression and delays mortality in a transgenic mouse model of Huntington disease. Nat Med 2000;6:797–801
6. Bracken MB, Shepard MJ, Collins WF, et al. A randomized, controlled trial of methylprednisolone or naloxone in the treatment of acute spinal-cord injury. Results of the Second National Acute Spinal Cord Injury Study. N Engl J Med 1990;322:1405–11
7. Popovich PG, Longbrake EE. Can the immune system be harnessed to repair the CNS? Nat Rev Neurosci 2008;9:481–93
8. Ankeny DP, Popovich PG. Mechanisms and implications of adaptive immune responses after traumatic spinal cord injury. Neuroscience 2009;158:1112–21
9. Donnelly DJ, Popovich PG. Inflammation and its role in neuroprotection, axonal regeneration and functional recovery after spinal cord injury. Exp Neurol 2008;209:378–88
10. Franzen R, Schoenen J, Leprince P, et al. Effects of macrophage transplantation in the injured adult rat spinal cord: A combined immunocytochemical and biochemical study. J Neurosci Res 1998;51:316–27
11. Rapalino O, Lazarov-Spiegler O, Agranov E, et al. Implantation of stimulated homologous macrophages results in partial recovery of paraplegic rats. Nat Med 1998;4:814–21
12. Rabchevsky AG, Streit WJ. Grafting of cultured microglial cells into the lesioned spinal cord of adult rats enhances neurite outgrowth. J Neurosci Res 1997;47:34–48
13. Prewitt CM, Niesman IR, Kane CJ, et al. Activated macrophage/microglial cells can promote the regeneration of sensory axons into the injured spinal cord. Exp Neurol 1997;148:433–43
14. Taoka Y, Okajima K. Role of leukocytes in spinal cord injury in rats. J Neurotrauma 2000;17:219–29
15. Kreutzberg GW. Microglia: A sensor for pathological events in the CNS. Trends Neurosci 1996;19:312–18
16. Popovich PG, Hickey WF. Bone marrow chimeric rats reveal the unique distribution of resident and recruited macrophages in the contused rat spinal cord. J Neuropathol Exp Neurol 2001;60:676–85
17. Ulvestad E, Williams K, Mørk S, et al. Phenotypic differences between human monocytes/macrophages and microglial cells studied in situ and in vitro. J Neuropathol Exp Neurol 1994;53:492–501
18. Shechter R, London A, Varol C, et al. Infiltrating blood-derived macrophages are vital cells playing an anti-inflammatory role in recovery from spinal cord injury in mice. PLoS Med 2009;6:e1000113
19. Schlueter AJ, Malek TR, Hostetler CN, et al. Distribution of Ly-6C on lymphocyte subsets: I. Influence of allotype on T lymphocyte expression. J Immunol 1997;158:4211–22
20. Davoust N, Vuaillat C, Androdias G, et al. From bone marrow to microglia: Barriers and avenues. Trends Immunol 2008;29:227–34
21. Priller J, Flugel A, Wehner T, et al. Targeting gene-modified hematopoietic cells to the central nervous system: Use of green fluorescent protein uncovers microglial engraftment. Nat Med 2001;7:1356–61
22. Wehner T, Bontert M, Eyupoglu I, et al. Bone marrow–derived cells expressing green fluorescent protein under the control of the glial fibrillary acidic protein promoter do not differentiate into astrocytes in vitro and in vivo. J Neurosci 2003;23:5004–11
23. Kigerl KA, Gensel JC, Ankeny DP, et al. Identification of two distinct macrophage subsets with divergent effects causing either neurotoxicity or regeneration in the injured mouse spinal cord. J Neurosci 2009;29:13435–44
24. Mildner A, Schmidt H, Nitsche M, et al. Microglia in the adult brain arise from Ly-6ChiCCR2+ monocytes only under defined host conditions. Nat Neurosci 2007;10:1544–53
25. Ajami B, Bennett JL, Krieger C, et al. Local self-renewal can sustain CNS microglia maintenance and function throughout adult life. Nat Neurosci 2007;10:1538–43
26. Guillemin GJ, Brew BJ. Microglia, macrophages, perivascular macrophages, and pericytes: A review of function and identification. J Leukocyte Biol 2004;75:388–97
27. Rotzius P, Soehnlein O, Kenne E, et al. ApoE(−/−)/lysozyme M(EGFP/EGFP) mice as a versatile model to study monocyte and neutrophil trafficking in atherosclerosis. Atherosclerosis 2009;202:111–18
28. Faust N, Varas F, Kelly LM, et al. Insertion of enhanced green fluorescent protein into the lysozyme gene creates mice with green fluorescent granulocytes and macrophages. Blood 2000;96:719–26
29. Markart P, Faust N, Graf T, et al. Comparison of the microbicidal and muramidase activities of mouse lysozyme M and P. Biochem J 2004;380:385–92
30. Oweida AJ, Dunn EA, Karlik SJ, et al. Iron-oxide labeling of hematogenous macrophages in a model of experimental autoimmune encephalomyelitis and the contribution to signal loss in fast imaging employing steady state acquisition (FIESTA) images. J Magn Reson Imaging 2007;26:144–51
31. Joshi M, Fehlings MG. Development and characterization of a novel, graded model of clip compressive spinal cord injury in the mouse: Part 1. Clip design, behavioral outcomes, and histopathology. J Neurotrauma 2002;19:175–90
32. Fleming JC, Norenberg MD, Ramsay DA, et al. The cellular inflammatory response in human spinal cords after injury. Brain 2006;129:3249–69
33. Jacob JE, Pniak A, Weaver LC, et al. Autonomic dysreflexia in a mouse model of spinal cord injury. Neuroscience 2001;108:687–93
34. Saville LR, Pospisil CH, Mawhinney LA, et al. A monoclonal antibody to CD11d reduces the inflammatory infiltrate into the injured spinal cord: A potential neuroprotective treatment. J Neuroimmunol 2004;156:42–57
35. Tacke F, Randolph GJ. Migratory fate and differentiation of blood monocyte subsets. Immunobiology 2006;211:609–18
36. Kerstens HM, Poddighe PJ, Hanselaar AG. A novel in situ hybridization signal amplification method based on the deposition of biotinylated tyramine. J Histochem Cytochem 1995;43:347–52
37. Bao F, Chen Y, Dekaban GA, et al. Early anti-inflammatory treatment reduces lipid peroxidation and protein nitration after spinal cord injury in rats. J Neurochem 2004;88:1335–44
38. Pandit TS, Sikora L, Muralidhar G, et al. Sustained exposure to nicotine leads to extramedullary hematopoiesis in the spleen. Stem Cells 2006;24:2373–81
39. Campanella M, Sciorati C, Tarozzo G, et al. Flow cytometric analysis of inflammatory cells in ischemic rat brain. Stroke 2002;33:586–92
40. Geissmann F, Jung S, Littman DR. Blood monocytes consist of two principal subsets with distinct migratory properties. Immunity 2003;19:71–82
41. Auffray C, Fogg D, Garfa M, et al. Monitoring of blood vessels and tissues by a population of monocytes with patrolling behavior. Science 2007;317:666–70
42. Williams K, Schwartz A, Corey S, et al. Proliferating cellular nuclear antigen expression as a marker of perivascular macrophages in simian immunodeficiency virus encephalitis. Am J Pathol 2002;161:575–85
43. Thomas WE. Brain macrophages: On the role of pericytes and perivascular cells. Brain Res 1999;31:42–57
44. Streit WJ, Graeber MB, Kreutzberg GW. Functional plasticity of microglia: A review. Glia 1988;1:301–7
45. Gray M, Palispis W, Popovich PG, et al. Macrophage depletion alters the blood-nerve barrier without affecting Schwann cell function after neural injury. J Neurosci Res 2007;85:766–77
46. Kubota A, Suzuki K. Effect of liposome-mediated macrophage depletion on Schwann cell proliferation during Wallerian degeneration. J Neurotrauma 2000;17:789–98

47. Randolph GJ, Jakubzick C, Qu C. Antigen presentation by monocytes and monocyte-derived cells. Curr Opin Immunol 2008;20:52–60
48. Bao F, Chen Y, Dekaban GA, et al. An anti-CD11d integrin antibody reduces cyclooxygenase-2 expression and protein and DNA oxidation after spinal cord injury in rats. J Neurochem 2004;90:1194–204
49. Youker KA, Beirne J, Lee J, et al. Time-dependent loss of Mac-1 from infiltrating neutrophils in the reperfused myocardium. J Immunol 2000;164:2752–58
50. Geremia NM, Bao F, Rosenzweig TE, et al. CD11d antibody treatment improves recovery in spinal cord–injured mice. J Neurotrauma [published online ahead of print December 20, 2011] doi:1089/neu.2011.1976
51. Ginhoux F, Greter M, Leboeuf M, et al. Fate mapping analysis reveals that adult microglia derive from primitive macrophages. Science 2010;330:841–45
52. Kigerl KA, McGaughy VM, Popovich PG. Comparative analysis of lesion development and intraspinal inflammation in four strains of mice following spinal contusion injury. J Comp Neurol 2006;494:578–94
53. Cross M, Mangelsdorf I, Wedel A, et al. Mouse lysozyme M gene: Isolation, characterization, and expression studies. Proc Natl Acad Sci U S A 1988;85:6232–36
54. Schilling M, Strecker JK, Ringelstein EB, et al. Turn-over of meningeal and perivascular macrophages in the brain of MCP-1-, CCR-2- or double knockout mice. Exp Neurol 2009;219:583–85
55. Chinnery HR, Ruitenberg MJ, McMenamin PG. Novel characterization of monocyte-derived cell populations in the meninges and choroid plexus and their rates of replenishment in bone marrow chimeric mice. J Neuropathol Exp Neurol 2010;69:896–909
56. Jordan FL, Thomas WE. Brain macrophages: Questions of origin and interrelationship. Brain Res 1988;472:165–78
57. Donnelly DJ, Longbrake EE, Shawler TM, et al. Deficient CX3CR1 signaling promotes recovery after mouse spinal cord injury by limiting the recruitment and activation of Ly6Clo/iNOS+ macrophages. J Neurosci 2011;31:9910–22
58. Polfliet MM, Goede PH, van Kesteren-Hendrikx EM, et al. A method for the selective depletion of perivascular and meningeal macrophages in the central nervous system. J Neuroimmunol 2001;116:188–95
59. Polfliet MM, van de Veerdonk F, Dopp EA, et al. The role of perivascular and meningeal macrophages in experimental allergic encephalomyelitis. J Neuroimmunol 2002;122:1–8
60. Qian Q, Jutila MA, Van Rooijen N, et al. Elimination of mouse splenic macrophages correlates with increased susceptibility to experimental disseminated candidiasis. J Immunol 1994;152:5000–8
61. Sroga JM, Jones TB, Kigerl KA, et al. Rats and mice exhibit distinct inflammatory reactions after spinal cord injury. J Comp Neurol 2003;462:223–40
62. Pineau I, Lacroix S. Proinflammatory cytokine synthesis in the injured mouse spinal cord: Multiphasic expression pattern and identification of the cell types involved. J Comp Neurol 2007;500:267–85
63. Pineau I, Sun L, Bastien D, et al. Astrocytes initiate inflammation in the injured mouse spinal cord by promoting the entry of neutrophils and inflammatory monocytes in an IL-1 receptor/MyD88–dependent fashion. Brain Behav Immun 2010;24:540–53
64. Toledo KA, Pereira FL, Mambole A, et al. The macrophage-derived neutrophil chemotactic factor, MNCF: A lectin with TNF-alpha–like activities on neutrophils. Biochem Biophys Res Commun 2008;376:764–69
65. Müller I, Munder M, Kropf P, et al. Polymorphonuclear neutrophils and T lymphocytes: Strange bedfellows or brothers in arms? Trends Immunol 2009;30:522–30
66. Taoka Y, Okajima K, Uchiba M, et al. Role of neutrophils in spinal cord injury in the rat. Neuroscience 1997;79:1177–82
67. Mantovani A, Sica A, Sozzani S, et al. The chemokine system in diverse forms of macrophage activation and polarization. Trends Immunol 2004;25:677–86
68. Varin A, Gordon S. Alternative activation of macrophages: Immune function and cellular biology. Immunobiology 2009;214:630–41
69. David S, Kroner A. Repertoire of microglial and macrophage responses after spinal cord injury. Nat Rev Neurosci 2011;12:388–99
70. Clausen BE, Burkhardt C, Reith W, et al. Conditional gene targeting in macrophages and granulocytes using LysMcre mice. Transgenic Res 1999;8:265–77
71. Goren I, Allmann N, Yogev N, et al. A transgenic mouse model of inducible macrophage depletion: Effects of diphtheria toxin-driven lysozyme M–specific cell lineage ablation on wound inflammatory, angiogenic, and contractive processes. Am J Pathol 2009;175:132–47